Yrast decay schemes from heavy-ion + ^{48}Ca fusion-evaporation reactions. III. ^{57,58}Fe, ^{54,55}Cr, and ^{57,58}Mn†

A. M. Nathan,* J. W. Olness, and E. K. Warburton
Brookhaven National Laboratory, Upton, New York 11973

J. B. McGrory‡
Oak Ridge National Laboratory, Oak Ridge, Tennessee 37830

(Received 8 November 1977)

Fusion-evaporation reactions induced by beams of 25–65 MeV ^{13}C, ^{15}N, ^{11}B, and ^{9}Be on an isotopically enriched ^{48}Ca target have been used to populate high-spin yrast levels in ^{57,58}Fe, ^{54,55}Cr, and ^{57,58}Mn. Measurements consisted of γ-ray excitation functions, angular distributions, γ-γ coincidences, and recoil-distance and Doppler shift lifetime measurements, from which were deduced the energy levels, γ-ray branching ratios, most probable spin-parity assignments, and level lifetimes. Comparision is made with a large-basis shell-model calculation.

[NUCLEAR REACTIONS ^{48}Ca(^{13}C, $xn, yp, z\alpha$)^{57,58}Fe, ^{54,55}Cr, and ^{57,58}Mn; ^{48}Ca(^{15}N, $\alpha 2n$)^{57}Mn; ^{48}Ca(^{11}B, pxn)^{54,55}Cr; and ^{48}Ca(^{9}Be, $3n$)^{54}Cr. E=25–65 MeV; measured $\sigma(E, E_\gamma)$ and coin; deduced levels; measured $\sigma(E_\gamma, \theta)$; deduced J^π for high-spin levels; measured RDM and Doppler shifts; deduced t_m, $|M(M1)|^2$, and $|M(E2)|^2$. Enriched targets, Ge(Li) detectors.]

I. INTRODUCTION

In this third of a series of reports of high-spin yrast decay schemes in nuclei formed by heavy-ion (HI) + ^{48}Ca fusion-evaporation reactions, we report on ^{57,58}Fe, ^{54,55}Cr, and ^{57,58}Mn. These nuclei were formed by the reactions ^{48}Ca(^{13}C, $3n$)^{58}Fe, ^{48}Ca(^{13}C, $4n$)^{57}Fe, ^{48}Ca(^{13}C, $\alpha 2n$)^{55}Cr, ^{48}Ca(^{13}C, $\alpha 3n$)^{54}Cr, ^{48}Ca(^{13}C, $p2n$)^{58}Mn, ^{48}Ca(^{13}C, $p3n$)^{57}Mn, ^{48}Ca(^{15}N, $\alpha 2n$)^{57}Mn, ^{48}Ca(^{11}B, $p3n$)^{55}Cr, ^{48}Ca(^{11}B, $p4n$)^{54}Cr, and ^{48}Ca(^{9}Be, $3n$)^{54}Cr.

The experimental investigations included γ-ray excitation functions and angular distributions, γ-γ coincidence spectra, and lifetime measurements via the Doppler-shift-attenuation method (DSAM) and recoil-distance method (RDM). These procedures, the data analysis methods, and criteria for establishing decay schemes and spin-parity assignments or preferences have been fully described in the first paper[1] of this series (hereafter referred to as I), to which the reader is referred for a more complete discussion and presentation. Whereas I described nuclei formed principally via ^{11}B + ^{48}Ca(^{54,56}Mn, ^{56}Cr, and ^{52,53}V), and II was focused on the nuclei ^{59,60}Fe and ^{59,60}Co as formed primarily via the ^{15}N + ^{48}Ca and ^{18}O + ^{48}Ca reactions,[2] the present paper deals with those nuclei observed strongly in ^{13}C + ^{48}Ca, with additional supporting data from other reactions as indicated above. In I we described the systematic dependence of ^{11}B + ^{48}Ca fusion-evaporation products on bombarding energy. The yield curves for ^{13}C + ^{48}Ca have the same general behavior, as is expected since the compound nuclei for ^{11}B and ^{13}C bombardment of ^{48}Ca ($^{59}_{25}$Mn$_{34}$ and $^{61}_{26}$Fe$_{35}$, respectively) are both neutron-rich ($T_z = \frac{9}{2}$) *vis a vis* the valley of stability. Thus neutron evaporation is favored over charged-particle emission. This

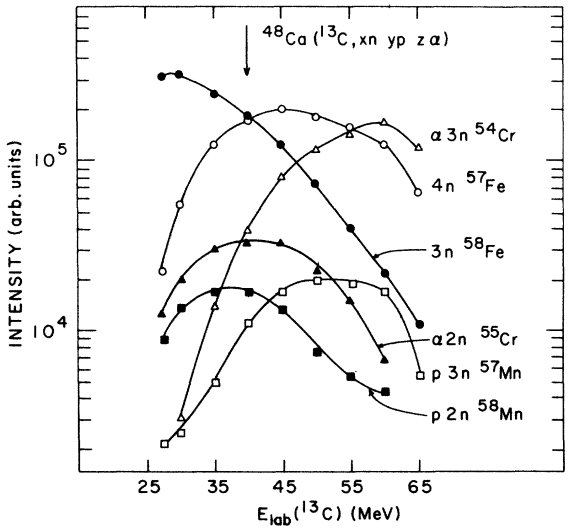

FIG. 1. Relative yield as a function of bombarding energy for the production of various final nuclei in the bombardment of ^{48}Ca with ^{13}C. The outgoing particles in the exit channel of the fusion-evaporation reaction are also identified.

is demonstrated in Fig. 1, which shows the 90°-yield curves for representative γ rays from each of the final nuclei studied with $^{48}Ca + ^{13}C$ from 27.5- to 65-MeV beam energy. We see that at 40 MeV, where the angular distribution, γ-γ coincidence, and RDM measurements were performed, $^{57,58}Fe$ were formed quite strongly, while $^{54,55}Cr$ were formed with medium strength and $^{57,58}Mn$ were formed with only weak-to-medium strength. $^{54,55}Cr$ were also formed with medium strength in $^{48}Ca + ^{11}B$ at 40 MeV and ^{54}Cr was formed quite strongly in $^{48}Ca + ^{9}Be$ at 27 MeV.

In the next section we present the decay schemes deduced from these data, and in the final section we discuss our results in the light of shell-model calculations performed in a large-basis configurational space. A composite listing of the γ rays observed in the reactions $HI + ^{48}Ca$ studied to date, prepared in a form similar to that presented in Table II of Ref. 1, is available upon request to one of the authors (E.K.W.).

II. DECAY SCHEMES

A. ^{57}Fe

^{57}Fe was formed in the $^{48}Ca(^{13}C, 4n)^{57}Fe$ reaction at beam energies between 27.5 and 65 MeV. The γ-ray energies, angular distributions, and Doppler-shift attenuation factors observed in this reaction at $E(^{13}C) = 40$ MeV are listed in Table I.

TABLE I. γ rays from ^{57}Fe observed in $^{48}Ca(^{13}C, 4n)^{57}Fe$ at $E(^{13}C) = 40$ MeV.

E_γ		Angular distribution [c]			
Present [a] (keV)	Previous [b]	I_γ	A_2 (%)	A_4 (%)	$F(\tau)$ [d]
121.97(3)	122.063(3) [e]	...	...	...	
136.48(*P*)	136.476(3) [e]	...	...	...	
230.27(14)	230.25(4)	2422	...	...	
256.03(11)	255.9(2)	229242	−30(1)	0	
339.60(*P*) [f]	339.60(6)	...	...	...	
352.21(10)	352.32(3) [e]	26443	3(3)	0	
366.65(12)	366.73(4)	5651	−52(15)	0	
379.06(13)	...	5720	−39(10)	0	0.98(2)
558.99(14)	...	10606	...	...	1.1(1)
640.20(14)	641	10968	9(5)	0	
650.49(15)	650.4(3)	13056	−63(5)	36(6)	
691.97(15)	692.00(3) [e]	50873	−44(2)	12(3)	
705.53(50) [g]	706.42(6) [e]	≤31027 [g]	−22(9)	−32(4)	0.72(4)
813.73(15)	...	79967	23(2)	−14(2)	<0.15
870.62(16) [g]	870.68(5) [e]	≤200909 [g]	−80(1)	14(11)	
913.37(16)	913.1(2)	163387	−38(1)	7(1)	<0.15
982.97(32)	982.3(4)	7283	...	...	
992.63(16)	992.68(8) [e]	102218	21(1)	−8(2)	0.15(5)
1061.60(17)	1061.3(2)	483892	21(1)	−7(1)	0.13(5)
1158.37(18)	1157.4(2)	112682	<0		>0
1256.27(19)	1256.0	178800	32(5)	−13(5)	0.54(10)
1282.85(27)	1282.0	...	...	...	
1297.78(52)	1295(2)	...	...	...	1.1(2)
1303.70(31)	...	...	...	...	>0
1348.86(19)	1348.8(3)	122127	25(2)	−12(2)	0.20(10)
1448.52(20)	1448.3(3)	89258	−31(3)	0	<0.15
1661.54(20)	...	131710	60(20)	−20(10)	1.0(1)
1680.58(21)	1680.9(3)	250057	32(1)	...	0.23(3)
2135.90(29)	...	≤85537 [g]	50(10)	−23(12)	0.9(1)

[a] Uncorrected for nuclear recoil. Numbers in parentheses are errors in the least significant figure and a *P* indicates the energy is taken from the literature.

[b] From the $^{54}Cr(\alpha, n\gamma)^{57}Fe$ reaction, Ref. 3, except where indicated.

[c] Results of fitting $^{13}C + ^{48}Ca$ angular distributions with the Legendre polynomial function $W(\theta) = I_\gamma[1 + A_2P_2(\cos\theta) + A_4P_4(\cos\theta)]$.

[d] The DSAM attenuation factor defined in Ref. 1.

[e] From the most recent compilation, Ref. 4.

[f] Observed in γ-γ coincidences only.

[g] Includes contribution from an unresolved contaminant; observed clearly in γ-γ coincidences only.

TABLE II. Energy levels, lifetimes, and γ-ray branching ratios and transition strengths for ^{57}Fe from the ^{48}Ca(^{13}C, $4n$)^{57}Fe reaction.

E_i [a] (keV)	E_f (keV)	E_γ (keV)	Branching ratio (%) Previous [b]	Present	J_i^π [c]	J_f^π	Mixing ratio δ [b] ($\times 100$)	Mean life [d] (ps)	Assumed multipole	$\lvert M\rvert^2$ (mW.u./W.u.) [e]
14.4127(4) [f]	0	14	100	...	$\frac{3}{2}^-$	$\frac{1}{2}^-$	...	142(1) ns [f]		
136.4768(24) [f]	14	122	88	...	$\frac{5}{2}^-$	$\frac{3}{2}^-$	0.120 ± 0.002	12.4(4) ns [f]		
	0	136	12	...		$\frac{1}{2}^-$			$E2$	12.7 ± 0.4
366.74(2) [f]	136	230	8	7(3)	$\frac{3}{2}^-$	$\frac{5}{2}^-$		14(3) [f] 17(2)		
	14	352	77	77(2)		$\frac{3}{2}^-$				
	0	367	15	16(3)		$\frac{1}{2}^-$				
706.407(23)	367	340	3	...	$\frac{5}{2}^-$	$\frac{3}{2}^-$		4.2(7) [f]		
	136	570 [g]	8	...		$\frac{5}{2}^-$	2.0 ± 2.3			
	14	692	85	...		$\frac{3}{2}^-$	−0.8 ± 0.4			
	0	706	4	...		$\frac{1}{2}^-$			$E2$	3.3 ± 1.6
1007.13(5)	367	640	...	3(2)	$\frac{7}{2}^-$	$\frac{3}{2}^-$				
	136	871	64	64(1)		$\frac{5}{2}^-$	$0.6^{+0.5}_{-0.2}$			
	14	993	36	33(1)		$\frac{3}{2}^-$				
1197.97(13)	136	1062	100	100	$(\frac{9}{2})^-$	$\frac{5}{2}^-$		4.2(5)	$E2$	10.8 ± 1.3
1356.87(13)	706	650	100	100	$\frac{7}{2}^-$	$\frac{7}{2}^-$	$0.3^{+0.2}_{-0.3}$ 1.6 ± 0.3			
1989.31(22)	1198	792 [g]	...	...	$\frac{9}{2}^{(-)}$	$(\frac{9}{2})^-$				
	1007	983	...	...		$\frac{7}{2}^-$	1.5 ± 1.3			
	706	1283	...	...		$\frac{5}{2}^-$				
2356.04(46)	1198	1158	30	48(4)	$(\frac{11}{2})^-$	$(\frac{9}{2})^-$	0.45 ± 0.05	<0.2	$M1$	>58
	1007	1349	70	52(4)		$\frac{7}{2}^-$			$E2$	>3.4
2455.61(26)	1007	1449	100	100	$(\frac{9}{2}^+)$ [h]	$\frac{7}{2}^-$	0.00 ± 0.04			
2878.70(20)	1198	1681	100	100	$(\frac{13}{2})^-$	$(\frac{9}{2})^-$		<0.2	$E2$	>22
3134.69(23)	2879	256	100	100	$(\frac{15}{2})$	$(\frac{13}{2})^-$	0.07 ± 0.02	231(10)	$M1$ $E2$	8.1 ± 0.4 1.1 ± 0.1

TABLE II. (*Continued*)

E_i [a] (keV)	E_f (keV)	E_γ (keV)	Branching ratio (%) Previous [b]	Present	J_i^π [c]	J_f^π	Mixing ratio δ [b] (×100)	Mean life [d] (ps)	Assumed multipole	$\lvert M\rvert^2$ (mW.u./W.u.) [e]
3269.40(29)	2456	814 [i]	···	33(2)	$(\frac{13}{2}^+)$	$(\frac{9}{2}^+)$		1.5–5	*E*2	11–36
	2356	913	100	67(2)		$(\frac{11}{2})^-$	0.00 ±0.03		*E*1	0.08–0.27
3513.79(32) [i]	3135	379	···	100	$(\frac{17}{2})$	$(\frac{15}{2})$		<0.2	*M*1	
4432.24(57)	3135	1298	100	100	$(\frac{17}{2})$	$(\frac{15}{2})$		<0.2	*M*1	
4525.75(36)	3269	1256	100	100	$(\frac{17}{2}^+)$	$(\frac{13}{2}^+)$		0.55(20)	*E*2	34 ±12
6187.32(41) [i]	4526	1662	···	100	$(\frac{21}{2}^+)$	$(\frac{17}{2}^+)$		<0.2	*E*2	>23.1
8323.26(50) [i]	6187	2136	···	100	$(\frac{25}{2}^+)$	$(\frac{21}{2}^+)$		<0.2	*E*2	>6.6

[a] Weighted means of energies deduced from the present γ-ray studies and the most recent $A=57$ compilation, Ref. 4. The correction for nuclear recoil has been made, and only levels deduced from the present work are listed. Except where indicated, all levels and γ-ray decay modes were previously observed in the $^{54}Cr(\alpha,n\gamma)^{57}Fe$ studies, Ref. 3.

[b] Except for the first four levels, these are from the $^{54}Cr(\alpha,n\gamma)^{57}Fe$ studies, Ref. 3. Otherwise they are from other work summarized in Ref. 4.

[c] The J^π for the lowest four levels are from $^{56}Fe(d,p)^{57}Fe$ studies, as compiled in Ref. 4. The others are deduced from a combination of the present data and the $^{54}Cr(\alpha,n\gamma)^{57}Fe$ studies, Ref. 3.

[d] The present results are from DSAM studies, except for the 367-, 1198-, and 3135-keV levels and the upper limit on the 3269-keV level, which are from the RDM.

[e] The units are W.u. for *E*2 and mW.u. for dipole transitions.

[f] Level energies and mean lives are from Ref. 4.

[g] Not observed in the present work.

[h] The positive-parity assignment follows from the $l=4$ stripping pattern observed in $^{56}Fe(d,p)^{57}Fe$.

[i] Previously unobserved.

The corresponding energy levels and γ-ray decay properties deduced for states in ^{57}Fe from these data are given in Table II and the decay scheme is shown in Fig. 2. The high-spin yrast cascade in ^{57}Fe had previously been studied by Sawa[3] utilizing in-beam γ-ray spectroscopy from the ^{54}Cr$(\alpha, n\gamma)^{57}$Fe reaction. The γ rays observed in that reaction are also listed in Table I; the energies agree quite well with the somewhat more precise values determined in the present work. All levels in Fig. 2 below 4600 keV were also observed by Sawa and except for the 814-keV transition (3269 → 2456), which was previously unassigned, the γ-ray decay scheme deduced for these levels by Sawa[3] is confirmed by the present results. The 6187- and 8323-keV levels were previously unobserved.

The lifetimes for the levels shown in Fig. 2 are given in Table II. For levels below 800 keV, the values are taken from the literature.[4] We have also measured the meanlife of the 367-keV level via the RDM on the 352-keV γ ray and the present result of 17 ± 2 ps agrees quite well with the previous value of 14 ± 3 ps. The remaining lifetimes are from the present DSAM and RDM results. For the levels at 4432, 6187, and 8323 keV, the observation of a full or nearly full Doppler shift [$F(\tau) > 0.8$, Table I] for the 1298-, 1662-, and 2136-keV γ rays allows the upper limit $\tau < 0.2$ ps, and from the observation of $F(\tau) = 0.5 \pm 0.1$ for the 1256-keV γ ray we infer $\tau = 0.55 \pm 0.20$ ps for the 4526-keV level. The relatively long mean life, $\tau = 231 \pm 10$ ps, for the 3135-keV level was obtained from the RDM measurement on the 256-keV transition, and the upper limit, $\tau < 5$ ps, for the 3269-keV level follows from the nonobservation of an unshifted component for the 913-keV γ ray at the closest RDM distance (35 μm). The lower limit $\tau > 1.5$ ps for this latter level follows from $F(\tau) < 0.2$. The upper limits, $\tau < 0.2$ ps, for the 2879- and 2356-keV levels follow from the DSAM after correcting for the cascade feeding from above. These latter two limits improve on the limits determined by Sawa[3] of <0.67 and <0.60 ps, respectively. Finally, the lifetime of the 1198-keV level follows from the RDM on the 1062-keV transition, taking due account of the slow cascade feeding through the 3135-keV level.

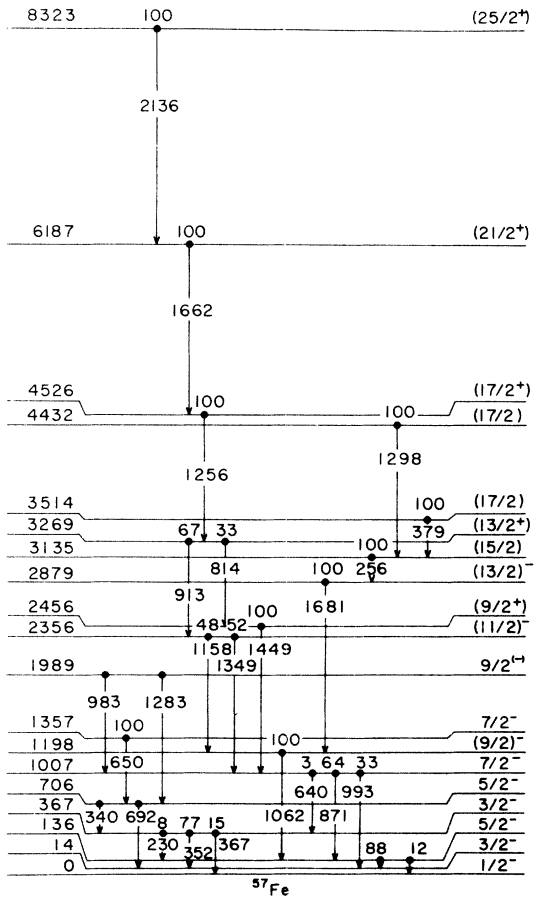

FIG. 2. Level scheme for ^{57}Fe deduced from present studies of the ^{48}Ca(^{13}C, $4n$)^{57}Fe reaction. Excitation energies and transition energies are in keV and branching ratios are in percent. Spin-parity assignments enclosed in parentheses indicate probable but uncertain conclusions, as discussed in the text.

The J^π assignments given in Table II for levels below 800 keV and for the 1357-keV level are mainly from (d, p) and Coulomb excitation studies[4]; those for the remaining levels below 3300 keV are from the (α, n) work of Sawa[3] and are confirmed by the present work. A convenient summary of these assignments may be found in the most recent compilation.[4] The J^π assignments suggested for the levels above 3300 keV are entirely from the present work.

Although we agree with and confirm the J^π assignments made by Sawa (with one exception noted below), we believe that several of these assignments adopted as definite[4] are based on nonrigorous methods and are sufficiently uncertain so that they should be placed in parentheses. In particular the γ-ray angular distributions were analyzed by assuming a Gaussian distribution of magnetic substate populations in the initial state, thus allowing a definite relationship between the A_2 and A_4 attenuation factors (α_2 and α_4, respectively).[3] However, this assumption is highly model-dependent and is unsubstantiated by existing data.[5,6] From a practical point of view, the absence of a relationship between α_2 and α_4 makes it nearly impossible on the basis of angular distributions alone to distinguish between a $J+2 \rightarrow J$

quadrupole transition and a $J \rightarrow J$ transition with dipole/quadrupole mixing ratio $\delta \approx -1.5$. Thus for example, in both the present data and that of Sawa, the angular distributions of the 1062-, 1349-, and 1681-keV transitions are consistent with both $J+2 \rightarrow J$ and $J \rightarrow J$. The γ-ray linear polarization data of Sawa rule out $J \rightarrow J$ for the 1681-keV transition; for the other cases the polarization data do not allow further restriction. However, $J+2 \rightarrow J$ is the most probable choice for all three transitions based on the argument that yrast states are selectively populated in these reactions. Since this argument is inherently nonrigorous, we enclose the indicated spin assignments for the 1198- and 2356-keV levels (and all higher levels that decay to these states) in parentheses. Negative parity for these levels and also the 2879-keV level are taken as definite, however, because of the nonzero A_4 coefficient for the γ rays depopulating these levels and the fact that the lifetimes are too fast[7] (see Table II) to allow any appreciable $M2$ component. We further note that the $\frac{7}{2}^-$ assignment to the 1007-keV level is also taken as definite since the positive A_2 and negative A_4 coefficient for the 993-keV transition to the $\frac{3}{2}^-$ level completely rules out the possibility that the transition is $\frac{5}{2} \rightarrow \frac{3}{2}$ or $\frac{3}{2} \rightarrow \frac{3}{2}$ while it is quite consistent with $\frac{7}{2} \rightarrow \frac{3}{2}$.

The one major uncertainty in the level scheme in Fig. 2 is the J^π assignment of the 2456-keV level. We identify this state with the level observed in high-resolution ^{56}Fe$(d,p)^{57}$Fe work,[8] at 2454 keV, which showed a strong $l=4$ stripping pattern thus implying $J^\pi = \frac{7}{2}^+$ or $\frac{9}{2}^+$. A subsequent $(\vec{d},p)$ vector-analyzing-power experiment confirmed $l=4$ but could not choose between $J = \frac{7}{2}$ and $\frac{9}{2}$.[9] The angular distribution of the 1449-keV (2456 → 1007) transition, as observed both in the present work and by Sawa, confirms the $J = \frac{7}{2}$ or $\frac{9}{2}$ assignment but provides no further restriction. However, the polarization experiment of Sawa favors odd parity but is consistent with all four possibilites $(J^\pi = \frac{7}{2}^\pm, \frac{9}{2}^\pm)$ at the two standard deviation limit. Since this latter study was not entirely conclusive, we favor $J^\pi = (\frac{9}{2}^+)$ as the most probable value. This choice is based on the (d,p) work and the shell model—which predicts that the lowest-lying $l=4$ transfer should be to a neutron $g_{9/2}$-orbital coupled to the 0^+ ^{56}Fe ground state.

The J^π assignments for higher-lying states depend on the J^π of the levels to which they decay. Figure 2 shows a sequence of four cascade transitions which terminate at the 2456-keV level, and the stretched quadrupole radiation pattern for these γ rays (see Table I) suggests $J = J_0+2$, J_0+4, J_0+6, and J_0+8 and $\pi = \pi_0$ for the 3269-, 4526-, 6187-, and 8323-keV levels, respectively, where $J_0^{\pi_0}$ is the spin-parity of the 2456-keV level. We will have more to say about this bandlike structure in the Discussion section (Sec. III).

Finally, we note that the 559-, 706-, and 1304-keV transitions, listed in Table I and assigned to ^{57}Fe from the γ-γ coincidence data, could not be placed into the decay scheme with any confidence and so are omitted from Fig. 2.

B. ^{58}Fe

The high-spin yrast cascade in ^{58}Fe was studied through the ^{48}Ca(^{13}C, $3n$)^{58}Fe reaction. A recent

TABLE III. γ rays from ^{58}Fe observed in ^{48}Ca(^{13}C, $3n$)-^{58}Fe at $E(^{13}\text{C}) = 40$ MeV.

E_γ [a] (keV)	I_γ	Angular distribution [b] A_2 (%)	A_4 (%)	$F(\tau)$ [c]
264.35(12)	16 920	−40(3)	0	<0.1
289.48(12)	61 600	30(2)	−8(3)	0.05(2)
454.73(14)	42 100	27(2)	−12(2)	<0.2
459.18(14)	18 400	−39(3)	9(3)	
466.27(14)	10 700	−65(5)	13(6)	
523.66(15)	35 200 [d]	10(2)	0	
782.84(16)	143 500 [d]	−28(3)	5(2)	<0.1
810.76(15)	491 900	19(2)	−6(2)	
863.89(16)	18 200	−22(6)	0	
925.71(20)	11 700 [d]	33(12)	0	
939.11(30)	58 200	<0	···	1.00(5)
959.16(40)	27 600	−22(5)	0	1.03(3)
1072.55(17)	62 500	−33(4)	0	
1162.64(18)	~158 000	41(6)	−13(5)	0.33(6)
1265.66(18)	374 100	21(3)	−8(4)	
1285.39(26)	~10 700	···	···	
1323.00(19)	43 100	−48(5)	29(10)	
1363.43(42)	~11 300	···	···	
1456.90(20)	~46 700	27(4)	−10(5)	
1520.45(20)	173 200	20(3)	0(2)	0.21(6)
1614.16(21)	42 300	−31(4)	10(4)	
1674.94(40)	~33 500	···	···	
1746.44(27)	~16 000	···	···	
1789.56(22)	24 800	18(5)	0	
1804.88(27)	4 800	···	···	
1809.87(22)	132 900	21(3)	−4(3)	
1897.7(10)	~105 000	20(3)	−15(5)	1.00(4) [e]
1906.0(10)	~25 000			
2138.22(40)	8 200	<0	···	
2340.7(20)	~44 000	45(14)	0	1.06(3)

[a] Uncorrected for nuclear recoil. Numbers in parentheses are errors in the least significant figure.

[b] Results of fitting ^{13}C + ^{48}Ca angular distributions with the Legendre polynomial function $W(\theta) = I_\gamma[1 + A_2 P_2(\cos\theta) + A_4 P_4(\cos\theta)]$.

[c] The DSAM attenuation factor defined in Ref. 1.

[d] Includes a small contribution from an impurity peak.

[e] These γ rays were not sufficiently resolved to allow a determination of their individual angular distributions. The results listed are for the sum of the two γ rays. The intensities are taken from the analysis of the γ-γ coincidence data and the yield curve data taken at 90°.

study of high-spin states in ^{58}Fe below 6 MeV has also been carried out by J. Delaunay *et al.*[10] using γ-ray techniques similar to ours but using the ^{55}Mn$(\alpha, p\gamma)^{58}$Fe reaction. However, the discussion below is based only on the present and previously published work, although we note that our results are generally consistent with the as yet unpublished results of Ref. 10.

The list of γ-ray energies, intensities, angular distributions, and Doppler-shift attenuation factors for γ rays from^{58}Fe observed in the present work at $E(^{13}\text{C}) = 40$ MeV is given in Table III. The corresponding energy levels, mean lives, and γ-ray decay properties deduced from these data for states in ^{58}Fe are given in Table IV, and the decay scheme, including feeding intensities, is shown in Fig. 3. Only the five levels below 2700 keV have been previously reported.[11] All information on these five levels in Table IV is taken from the 1976 compilation.[11]

The J^π assignments for the remaining levels rely heavily on the angular distribution information contained in Table III and the lifetime results, which were obtained mainly from the DSAM but also from RDM studies. The corresponding reduced transition rates are listed in Table IV. The $J^\pi = (6^+)$ suggestion for the 3597-keV level follows from the $J+2 \rightarrow J$ character of the angular distribution of the 1520-keV transition to the 2077-keV 4^+ level. However, as discussed above with regard to ^{57}Fe, a $J \rightarrow J$ transition, although not favored by the reaction mechanism, cannot be rigorously ruled out, and we therefore enclose the assignment in parentheses. We remark, however, that the nonappearance of a 4^+ level at 3597 keV in light ion-induced reactions supports

TABLE IV. Energy levels, lifetimes, and γ-ray branching ratios and transition strengths for ^{58}Fe from the ^{48}Ca(^{13}C, $3n$)^{58}Fe reaction.

E_i [a] (keV)	E_f (keV)	E_γ (keV)	Branching ratio (%)	J_i^π	J_f^π	Mean life (ps)	$B(E2)$ [b] (W.u.)
810.764(15)	0	811	100	2^+	0^+	11.7(2.3)	14.6(2.9)
1674.698(15)	0	1675	44	2^+	0^+		
	811	864	56		2^+		
2076.52(4)	811	1266	100	4^+	2^+		
2133.89(4)	811	1323	73	3^+	2^+		
	1674	459	27		2^+		
2600.39(4)	811	1790	30	$(4)^+$	2^+		
	1674	926	18		2^+		
	2077	524	39		4^+		
	2134	466	13		3^+		
2864.74(13)	2600	264	100	(5)	$(4)^+$	4.5(2.0)	10400(4600)
3596.99(20)	2077	1520	100	(6^+)	4^+	<4	>1.8
3886.45(22)	2077	1810	65	(6^+)	4^+	17(2)	0.12(1)
	2600	1285	5		$(4)^+$		0.05(1)
	3597	289	30		(6^+)		8900(1050)
4214.57(21)	2077	2138	16	(5) [c]	4^+		
	2600	1614	84		$(4)^+$		
4669.38(22)	2865	1805	2	(7) [c]	(5)		
	3597	1073	25		(6^+)		
	3886	783	56		(6^+)		
	4215	455	17		(5)		
5343.41(28)	3597	1746	26	(8^+)	(6^+)		
	3886	1457	74		(6^+)		
5503.0(14)	3597	1906	100	$[8^+]$	6^+	<0.2	
5832.03(28)	4669	1163	100	(9) [c]	(7)	1.1(4)	26(9)
6282.53(41)	5343	939	100	(9)	(8^+)	<0.2	>409
7242.69(57)	6283	959	100	(10)	(9)	<0.2	>368
7729.76(104)	5832	1898	100	(11) [c]	(9)	<0.2	>12
10070.5(22)	7730	2341	100	(13) [c]	(11)	<0.2	>4

[a] From the present γ-ray energies, after correcting for recoil. All information on levels with $E_x < 2700$ keV is taken from the literature as summarized in Ref. 11.

[b] Deduced from the mean life and branching ratio information, assuming the transitions are entirely electric quadrupole.

[c] The parity of these levels is the same as that of the 4669-keV level, for which there is weak evidence that $\pi = +$, as discussed in the text.

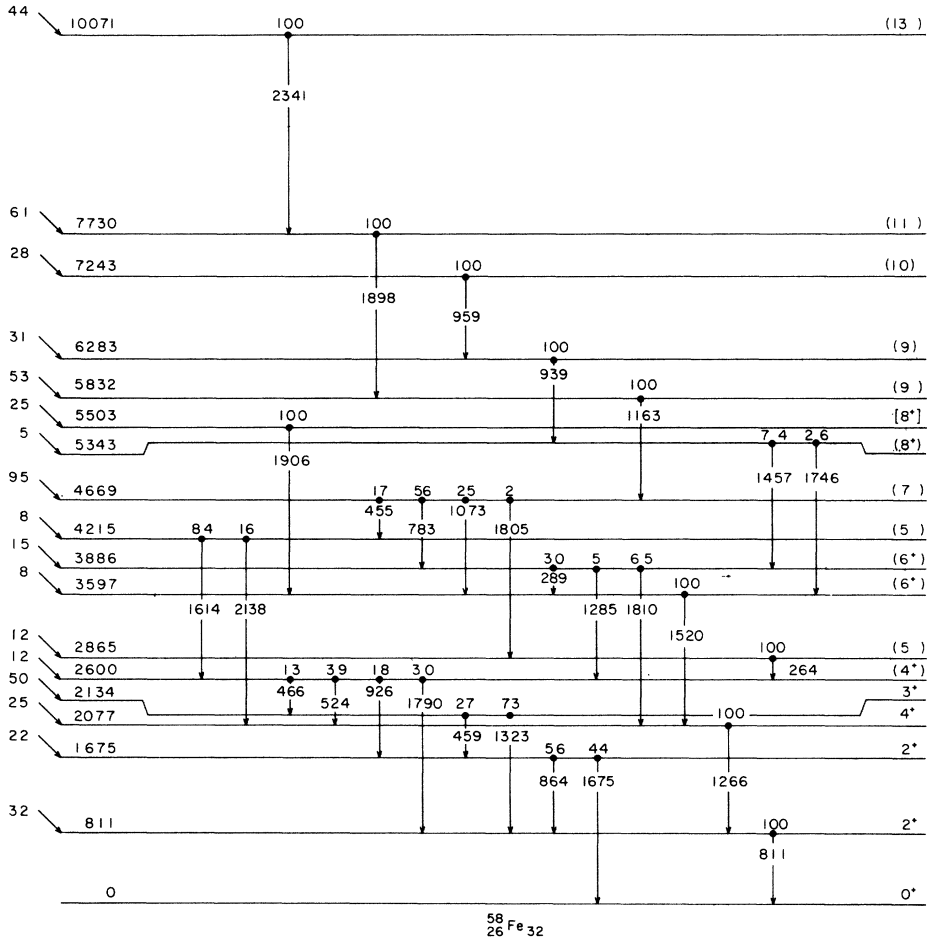

FIG. 3. Level scheme for ^{58}Fe deduced from the present studies of the ^{48}Ca(^{13}C, $3n$)^{58}Fe reaction. The notation is the same as in Fig. 2. In addition feeding intensities for direct population of various levels at $E(^{13}\mathrm{C}) = 40$ MeV are indicated on the far left. Square brackets designate J^{π} possibilities set forth as little more than a suggestion or working hypothesis. The parities of the 4215- and 4669-keV levels, as well as those levels that cascade through them, are all the same: weak evidence suggests $\pi = +$, as discussed in the text.

our contention that this is indeed a high-spin state. Similar radiation patterns ($A_2 > 0$, $A_4 < 0$) are observed for the 3886 → 2077 and 3886 → 3597 transitions. However, while we believe the first of these to be a stretched quadrupole transition, the lifetime of the 3886-keV level deduced from the RDM data is sufficient to assure that the second of these is predominantly dipole,[7] hence $J \rightarrow J$. These results thus yield an assignment of $J^{\pi} = (6^+)$ for the 3886-keV level. For the 4669-keV level, the characteristic $J+1 \rightarrow J$ dipole patterns for the 783- and 1073-keV transitions to the two (6^+) levels implies a $J = (7)$ assignment. The $J+2 \rightarrow J$ nature of the 4669 → 4215 transition then yields $J = (5)$ for this latter state. Positive parity for both these levels is suggested by the fact that a low-energy quadrupole transition (4669 → 4215) would not often compete favorably with $E1$ transitions (i.e., $7^- \rightarrow 6_1^+$ and $7^- \rightarrow 6_2^+$). Further support comes from the small but nonzero A_4 coefficients for both the 4669 → 3886 $[J^{\pi} = 6^+]$ and 4215 → 2600 $[J^{\pi} + 4^+]$ transitions. However, this latter argument is weakened somewhat by possible systematic uncertainties in the A_4 coefficients, while the former argument is, of course, inherently weak (although suggestive). Therefore, we do not make definite parity assignments to these levels, although it would seem that even parity is more likely.

Most of the intense direct feeding into ^{58}Fe in this reaction proceeds through the 10071 → 7730 → 5832 → 4669 $[J = (7)]$ cascade. These transitions all display strong Doppler shifts and exhibit stretched quadrupole radiation patterns. Accordingly, we assign $J^{\pi} = (13^{\pi_0})$, (11^{π_0}), and (9^{π_0}) to the upper three levels in this cascade, where

π_0 is the parity of the 4669-keV level. Another somewhat more weakly fed band consists of the 7243 → 6283 → 5343 → 3886 [$J^\pi = (6^+)$] cascade. The angular distribution of the last transition implies $J^\pi = (8^+)$ for the 5343-keV level. Unfortunately the 1746-keV γ ray from the decay of this level to the (6^+) state at 3597-keV was too weak to provide confirming evidence for this assignment. For the upper two levels of this cascade, the lifetimes and angular distributions for the 959- and 939-keV γ rays assure that these are mainly dipole transitions, and we therefore assign $J = (9)$ and (10) to the 6283- and 7243-keV levels, respectively. Similarly the 2865 → 2600 transition is dipole and hence $J = (5)$ for the upper level. Finally, the available information on the 5503-keV level is rather scanty since the primary γ decay via the 1906-keV transition to the 3597-keV(6^+) level is unresolved from the more intense 1898-keV γ ray. The angular distribution of the unresolved doublet is consistent with stretched quadrupole and based on this we give a $J^\pi = [8^+]$ assignment. The brackets, as discussed in I, reflect the scanty evidence upon which the assignment is based.

C. ^{54}Cr

^{54}Cr was studied in the present work mainly with the ^{48}Ca(^{9}Be, $3n$)^{54}Cr reaction at 27-MeV beam energy. Some redundant and consistent information was also obtained from the ^{48}Ca(^{13}C, $\alpha 3n$)^{54}Cr and ^{48}Ca(^{11}B, $p4n$)^{54}Cr reactions, and a concurrent study of the β-delayed γ-ray activity from ^{48}Ca(^{9}Be, $p2n$)^{54}V(β^-)^{54}Cr has already been reported.[12] The γ-ray decay information is gathered in Table V, and the decay scheme deduced from these data is shown in Fig. 4. Additional γ rays from the decay of non-yrast levels populated in ^{54}V(β^-)^{54}Cr (Ref. 12) are not shown in Table V or Fig. 4.

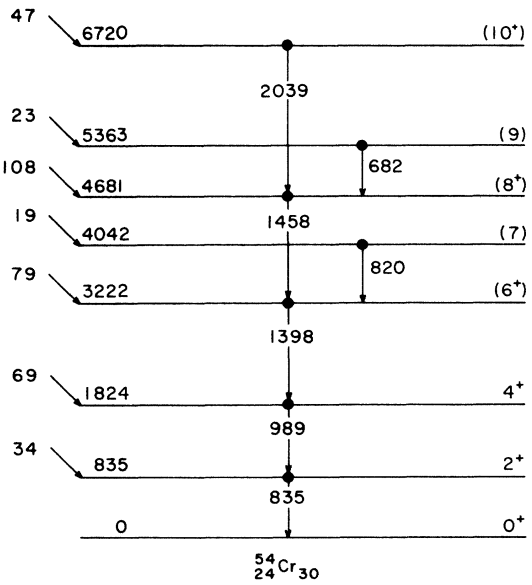

FIG. 4. Level scheme for ^{54}Cr deduced mainly from present studies of the ^{48}Ca(^{9}Be, $3n$)^{54}Cr reaction. Direct feeding intensities for $E(^9\text{Be}) = 27$ MeV are indicated on the far left. The notation is the same as in Fig. 2.

Only the three levels below 3300 keV have been reported previously.[12,13] The $J^\pi = 2^+$ and 4^+ assignments to the first two of these levels are from the literature.[13] The $J^\pi = (6^+)$, (8^+), and (10^+) suggestions for the levels at 3222, 4681, and 6720 keV, respectively, follow from the 4^+ assignment to the 1824-keV level and the $J+2 \rightarrow J$ character of the angular distributions of the 1398-, 1458-, and 2039-keV transitions. The intense side feeding into these levels supports these assign-

TABLE V. Decay scheme for high-spin states in ^{54}Cr deduced from the ^{48}Ca(^{9}Be, $3n$)^{54}Cr reaction at $E(^9\text{Be}) = 27$ MeV. The theoretical calculations for the $B(E2)$'s are described in the text.

			Angular distribution							$B(E2)$	
E_i [a] (keV)	E_f (keV)	E_γ (keV)	I_γ	A_2 (%)	A_4 (%)	$F(\tau)$	τ [b] (ps)	J_i^π	J_f^π	Exp. (W.u.)	Theor. (W.u.)
834.86(5) [c]	0	834.80(10)	3787	27(2)	−1(2)	<0.05	12.0(7) [c]	2^+	0^+	13.5(8) [c]	16.9
1823.89(15)	835	989.07(10)	3451	28(2)	−3(2)	0.06(1)	12(2) [c]	4^+ [c]	2^+	6(1) [c]	21.1
							2.8(8)			25(7)	
3222.33(18)	1824	1398.42(10)	2757	29(2)	−3(2)	0.29(3)	0.7(2)	(6^+)	4^+	18(5)	18.5
4042.28(26)	3223	819.94(19)	188	0 [d]	···	0.90(5)	<0.17	(7)	(6^+)	···	···
4680.57(23)	3223	1458.22(15)	1783	36(2)	−5(2)	0.44(4)	0.8(1)	(8^+)	(6^+)	12(2)	19.2
5362.70(28)	4683	682.13(16)	225	0 [d]	···	0.67(5)	0.35(8)	(9)	(8^+)	···	···
6719.52(79)	4683	2038.91(75)	474	29(4)	0	1.00(5)	<0.15	(10^+)	(8^+)	>12	14.2

[a] From the present γ-ray energies, corrected for nuclear recoil. All γ-ray decay branches are 100%.
[b] Mean life deduced from the $F(\tau)$ values in the previous column.
[c] From the Nuclear Data Group (unpublished).
[d] Angular distribution is consistent with isotropy.

ments. The observation of Doppler shifts for the 989-, 1398-, 1458-, 2039-keV γ rays allows lifetime determinations via the DSAM and these are included in Table V. Corrections were made for cascade feeding through the yrast levels and for slow feeding via $^{54}V(\beta^-)^{54}Cr$. Note that the mean-life deduced for the 1824-keV level ($\tau = 2.8 \pm 0.8$ ps) is in disagreement with the tabulated value of 12 ± 2 ps.[13] Regardless of this discrepancy, the picture of the ^{54}Cr yrast cascade that emerges from the present studies is that of a relatively enhanced [$B(E2) = 12-25$ W.u. (Weisskopf units)] $\Delta J = 2$ ground-state band extending up to the $J^\pi = (10^+)$ level at 6720 keV.

The levels at 4042 and 5363 keV were formed relatively weakly and it was not possible to obtain unambiguous angular distributions for the 820- and 682-keV γ rays. However, the lifetimes determined by analysis of the attenuated Doppler shifts is sufficient to assure that these transitions are predominantly dipole.[7] The reaction mechanism then favors assignments of $J = (7)$ and (9) for these two levels.

D. ^{55}Cr

^{55}Cr was formed in the $^{48}Ca(^{11}B, p3n)^{55}Cr$ and $^{48}Ca(^{13}C, \alpha 2n)^{55}Cr$ reactions at 35- and 40-MeV bombarding energy, respectively. A concurrent study of the β-delayed γ-ray activity from $^{48}Ca(^9Be, pn)^{55}V(\beta^-)^{55}Cr$ has already been reported.[12] The complete list of γ rays from these reactions, as deduced from the γ-ray yield curves and γ-γ coincidence data, is given in Table VI, including γ-ray energies and intensities, angular distribution coefficients, and Doppler-shift-attenuation factors $F(\tau)$. The level scheme deduced from these data is shown in Fig. 5 and summarized in Table VII. Only levels observed in the present γ-ray experiments are shown. All states with $E_x < 2100$ keV have been previously reported[14] with the exception of the 1479-keV level. Decays from all states with $E_x < 1500$ keV were observed in $^{55}V(\beta^-)^{55}Cr$ as well as in the in-beam studies, and the identification of levels with $E_x < 2100$ keV with

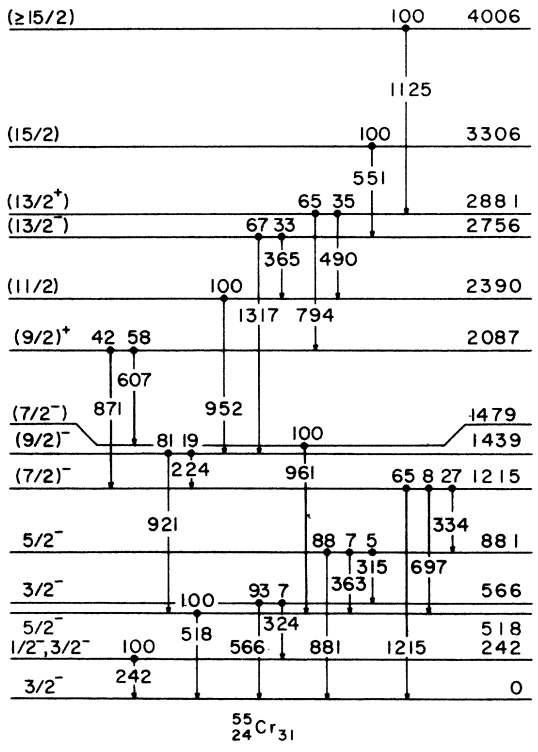

FIG. 5. Level scheme for ^{55}Cr deduced from present studies of the $^{48}Ca(^{11}B, p3n)^{55}Cr$ and $^{48}Ca(^{13}C, \alpha 2n)^{55}Cr$ reactions. The notation is the same as in Fig. 2.

TABLE VI. γ rays from ^{55}Cr observed in $^{48}Ca(^{11}B, p3n)^{55}Cr$, $^{48}Ca(^{13}C, \alpha 2n)^{55}Cr$, and $^{55}V(\beta^-)^{55}Cr$. Uncertainties in the least significant figure are enclosed in parentheses.

E_γ [a] (keV)	I_γ	Angular distribution [b] A_2 (%)	A_4 (%)	$F(\tau)$ [c]
224.08(8)	12 353	−38(3)	7(4)	
242.08(11)	~1 000	...	...	
314.81(10)	<3 400 [d]	...	...	
324.0(10)	~1 000	...	...	
334.06(8)	12 712	−26(3)	0	
363.05(10)	...	...	...	
365.10(12)	4 998	−19(17)	0	<0.2
489.96(12)	14 503	−32(3)	0	<0.2
517.77(10)	72 241	−37(1)	0	
550.73(14)	10 734	−46(4)	0	0.15(5)
565.90(13)	4 834	...	...	
607.12(12)	14 840 [e]	−18(5)	0	
696.92(24) [d]	~5 000 [d]	...	...	
794.25(12)	27 725	14(2)	0	<0.2
871.25(16)	10 680 [e]	...	...	
880.65(15)	10 431	−34(15)	0	
921.06(15)	48 010	37(3)	−10(3)	
951.61(15)	15 979	−48(20)	0	
961.39(20)	≤17 627 [d]	−43(7)	0	<0.3
1125.03(15)	21 121	...	...	<0.5
1214.76(12)	20 041	18(3)	0	
1316.60(20)	32 162	33(6) [e]	0	<0.3

[a] Mean values from $^{13}C + ^{48}Ca$, $^{11}B + ^{48}Ca$, and $^{55}V(\beta^-)^{55}Cr$.

[b] Results of fitting the $^{13}C + ^{48}Ca$ angular distributions with the Legendre polynomial function $W(\theta) = I_\gamma[1 + A_2P_2(\cos\theta) + A_4P_4(\cos\theta)]$. Cases with $A_4 = 0$ show no significant improvement in the fit with the inclusion of a P_4 term.

[c] The DSAM attenuation factor defined in Ref. 1.

[d] Includes contribution from an unresolved contaminant, observed cleanly in γ-γ coincidences only.

[e] Taken from the $^{11}B + ^{48}Ca$ data due to a contaminant γ ray in the $^{13}Ca + ^{48}Ca$ data.

TABLE VII. ^{55}Cr energy levels, lifetimes, and γ-ray transitions deduced from ^{48}Ca(^{11}B,$p3n$)^{55}Cr, ^{48}Ca(^{13}C,$\alpha 2n$)^{55}Cr, and ^{55}V(β^-)^{55}Cr.

E_i (keV) Present[a]	E_i (keV) Previous[b]	E_f (keV)	E_γ (keV)	Branching ratio (%) Previous[b]	Branching ratio (%) Present[c]	Assignments of J_i^π Previous[d]	Assignments of J_i^π Present[e]	J_f^π	Mean life (ps)
242.08(11)	241.86(4)	0	242	100	...	$\frac{1}{2}^-, \frac{3}{2}^-$	$\frac{1}{2}^-, \frac{3}{2}^-$	$\frac{3}{2}^-$	...
517.77(10)	517.68(5)	0	518	100	100	$\frac{5}{2}^-, \frac{7}{2}^-$	$\frac{5}{2}^-$	$\frac{3}{2}^-$	<7.5[f]
565.90(13)	565.90(4)	0	566	86	93(7)	$\frac{3}{2}^-$	$\frac{3}{2}^-$	$\frac{3}{2}^-$	...
		242	324	14	7(7)			$\frac{1}{2}^-, \frac{3}{2}^-$	
880.73(10)	880.75(9)	0	881	87	88(1)	$\frac{5}{2}^-, \frac{7}{2}^-$	$\frac{5}{2}^-$	$\frac{3}{2}^-$	...
		518	363	4	7(1)			$\frac{5}{2}^-$	
		566	315	9	5(1)			$\frac{3}{2}^-$	
1214.77(10)	1213(10)	0	1215	59	65(6)	$\frac{5}{2}^-, \frac{7}{2}^-$	$(\frac{7}{2})^-$	$\frac{3}{2}^-$	5^{+10}_{-2}[f]
		518	697	9	8(4)			$\frac{5}{2}^-$	
		881	334	32	27(5)			$\frac{5}{2}^-$	
1438.84(14)	1447(20)[g]	518	921	...	81(3)	$\frac{5}{2}^- - \frac{9}{2}^-$[d]	$(\frac{9}{2})^-$	$\frac{5}{2}^-$	6.0 ± 2.0[f]
		1215	224	...	19(3)			$(\frac{7}{2})^-$	
1479.17(22)	...	518	961	...	100	$(\frac{3}{2}^- - \frac{9}{2}^-)$[d]	$(\frac{7}{2}^-)$	$\frac{5}{2}^-$	...
2086.74(22)	2078(10)	1215	871	...	42(5)	$\frac{7}{2}^+, \underline{\frac{9}{2}^+}$	$(\frac{9}{2})^+$	$(\frac{7}{2})^-$	...
		1479	607	...	58(5)	...	$(\frac{11}{2})$	$(\frac{7}{2}^-)$	...
2390.46(22)	...	1439	952	...	100	...	$(\frac{11}{2})$	$(\frac{9}{2})^-$	...
2755.50(28)	...	1439	1317	...	67(5)	...	$(\frac{13}{2}^-)$	$(\frac{9}{2})^-$	<5
		2390	365	...	33(5)			$(\frac{11}{2})$	
2880.71(35)	...	2087	794	...	65(3)	...	$(\frac{13}{2}^+)$	$(\frac{9}{2})^+$	...
		2390	490	...	35(3)			$(\frac{11}{2})$	
3306.23(31)	...	2756	551	...	100	...	$(\frac{15}{2})$	$(\frac{13}{2}^-)$	3 ± 2[h]
4005.75(38)	...	2881	1125	...	100	...	$\geq \frac{15}{2}$	$(\frac{13}{2}^+)$	$0.5 < \tau < 3.0$[f,h]

[a] Deduced from the γ-ray energies of Table I, including corrections for nuclear recoil. The figures in parentheses are the uncertainties in the least significant figure. Only presently observed levels are included.

[b] From results summarized in the most recent compilation, Ref. 14.

[c] Utilizes γ-ray intensities from all three reactions.

[d] From the stripping patterns observed in ^{54}Cr(d,p) and ^{55}Cr(t,p) as compiled in Ref. 14, except where indicated. Underlined values indicate assignments preferred by the J dependence of (d,p) cross sections or the shell model.

[e] Utilizes the ^{55}V(β)^{55}Cr results of Ref. 12 as well as the previous restrictions (column 7).

[f] From the present RDM data.

[g] The listed uncertainty of ±20 keV is our estimate.

[h] From the present DSAM data.

previously observed levels (column 2 of Table VII) was discussed.[12] The levels with $E_x > 2100$ keV are assumed to be previously unobserved. The γ-ray decay modes obtained from the three reactions (column 6 of Table VII) are seen to be in fair agreement with previous results.[14]

The mean life information is summarized in Table VII. The lifetime obtained for the 3306-keV level was deduced from the $F(\tau)$ measurement on the 551-keV γ ray (see Table VI). No other γ rays showed a measurable Doppler shift. The mean lives of the 1215- and 1439-keV levels are from the RDM measurements on the 1215- and 921-keV γ rays, respectively. In obtaining these lifetimes it was assumed that the feeding from higher-lying states had negligible effect (Fig. 5); however, the uncertainties incorporate the possible influence of this feeding. For the 518-keV level, cascade feeding was also neglected and in this case the possible influence of this feeding is strong enough so that the resulting mean life is only an upper limit. For the 4006-keV level, the absence

of a Doppler shift results in a lower limit for the mean life while the nonobservation of an unshifted peak in the RDM measurements results in an upper limit. Because of the relatively low cross section for the formation of ^{55}Cr in both ^{11}B + ^{46}Ca and ^{13}C + ^{48}Ca it was not possible to obtain any other lifetimes.

The J^π assignments of $\frac{3}{2}^-$ for the ground state and 566-keV level and the $\frac{1}{2}^-$, $\frac{3}{2}^-$ possibilities for the 242-keV level are from previous studies.[14] Likewise, the levels at 518, 881, and 1215 keV were all observed to have an $l=1$ stripping pattern in ^{54}Cr$(d,p)^{55}$Cr so that $J^\pi = \frac{5}{2}^-$ or $\frac{7}{2}^-$ [14,16] Since $A_2 < 0$ for the 518 → 0 and 881 → 0 transitions, $J+2 \rightarrow J$ is rigorously ruled out and therefore $J^\pi = \frac{5}{2}^-$ for the 518- and 881-keV levels. In addition, the lifetime limit for the 518-keV level corresponds to an $E2$ strength of >230 W.u. (Ref. 5) and since this is unreasonably large[7] we have a further argument that the 518 → 0 transition is predominantly dipole. For the 1215-keV level, the intense direct feeding suggests an yrast level and therefore $J^\pi = (\frac{7}{2})^-$; this is supported by the angular distribution of the 1215 → 0 transition which is consistent with $J+2 \rightarrow J$.

We identify the 1439-keV level with the level at 1447 keV assigned an $L=4$ double-stripping pattern in ^{53}Cr$(t,p)^{55}$Cr. The intensities and angular distributions of the γ rays feeding and deexciting this level lead us to choose $J^\pi = \frac{9}{2}^-$ from the possibilities $\frac{5}{2}^- - \frac{11}{2}^-$ allowed by the $L=4(t,p)$ pattern. $J^\pi \geq \frac{11}{2}$ is also ruled against by the ^{55}V β-decay results.[12] The level at 2087 keV can probably be identified with the level assigned $l=4$ (and therefore $J^\pi = \frac{7}{2}^+$ or $\frac{9}{2}^+$) in the ^{54}Cr$(d,p)^{55}$Cr reaction. The shell model favors $\frac{9}{2}^+$ since this is expected from coupling a $g_{9/2}$ neutron to the ^{54}Cr ground state. If we accept this assignment, then the 1479-keV level has $J=\frac{7}{2}$ since the 2087 $(\frac{9}{2}^+)$ → 1479 → 518 $(\frac{5}{2}^-)$ cascade proceeds via γ rays that are at least partially dipole ($A_2 < 0$). The odd-parity suggestion for the 1479-keV level is the most likely explanation for the logft of 6.16 observed for the decay of ^{55}V to this level.[12]

For levels with $E_x > 2100$ keV, the J^π assignments follow from the direct feeding intensities, the consistency of the 1317-, 794-, and 1125-keV angular distributions with those expected for $J+2 \rightarrow J$ transitions, and the fact that the 952-, 365-, and 490-, and 551-keV transitions are at least partially dipole ($A_2 < 0$).

E. ^{57}Mn

^{57}Mn was formed, albeit weakly, in both the ^{48}Ca(^{13}C, $3np$)^{57}Mn and ^{48}Ca(^{15}N, $3n\alpha$)^{57}Mn reactions. The ^{57}Mn γ-γ coincidence scheme was

TABLE VIII. Decay scheme for high-spin states in ^{57}Mn deduced from the ^{48}Ca(^{13}C, $3np$)^{57}Mn reaction at $E(^{13}\text{C}) = 40$ MeV.

E_i [a] (keV)	E_f (keV)	E_γ (keV)	Angular distribution [b] I_γ	A_2 (%)	Branching ratio Present (%)	Previous [c] (%)	$F(\tau)$ [d]	τ [e] (ps)
83.26(20)	0	83.10(10)	~40 000	···	100	100	···	
1075.21(31)	0	1075.20 [f]	···	···	···	6	···	
	83	991.95 [f]	···	···	···	94	···	
1227.56(26)	83	1144.29(17)	35 338	21(5)	92(1)	94	<0.30	>0.5
	1075	152.35(16) [g]	3 036	···	8(1)	6	···	
2758.48(40)	1228	1530.92(30)	18 620	···	100	···	>0.2	<2.0
3287.33(45)	2758	528.85(20)	7 888	−39(8)	100	···	0.45(5)	0.7 ± 0.2
4710.4(1.0)	3287	1423.00(90) [h]	~3 000	···	100	···	>0.7	<0.4
?	≥1228	390.26(10)	3 808					
?	≥3287	671.9(2.0) [i]						
?	≥3287	785.8(2.0) [i]						

[a] From the γ-ray energies of column 3 including the nuclear recoil correction. The numbers in parentheses throughout the table are the uncertainties in the least significant figure.

[b] The γ-ray angular distribution is given by $W(\theta) = I_\gamma[1 + A_2 P_2(\cos\theta) + A_4 P_4(\cos\theta)]$. The A_4 coefficients were not determined with sufficient accuracy to distinguish them from zero.

[c] Reference 18.

[d] The DSAM attenuation factor defined in Ref. 1.

[e] Lifetimes derived from the $F(\tau)$ values.

[f] Not observed. The energies are calculated from the level separations.

[g] The assignment of this γ ray is uncertain. The energy given for the 1075-keV level is based on the energy of the 1228 → 1075 transition and is thus also uncertain.

[h] From ^{48}Ca(^{15}N, $2n\alpha$)^{57}Mn.

[i] Observed in coincidence only.

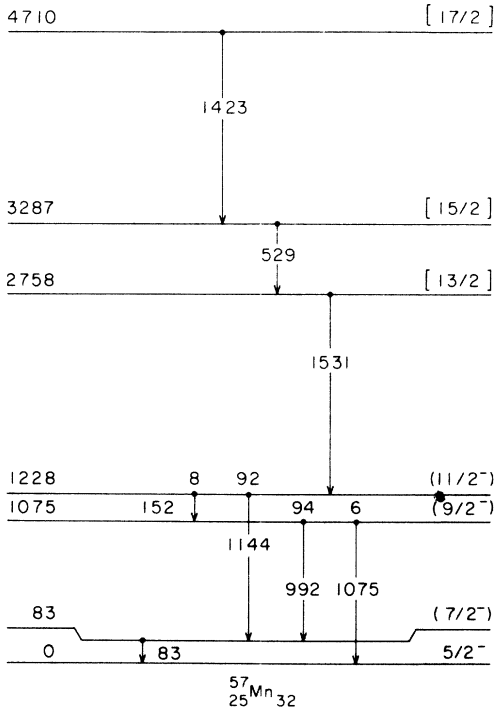

FIG. 6. Level scheme for ^{57}Mn deduced from studies of the ^{48}Ca(^{13}C, $3np$)^{57}Mn and ^{48}Ca(^{15}N, $3n\alpha$)^{57}Mn reactions, incorporating also the results from previous studies on the three lowest-lying levels. The notation is the same as in Fig. 2.

identified as such by the excitation functions and relative yields for the different projectiles from $A = 9$ to 18 and by the intensity balance with the β^- decay[17] to ^{57}Fe. The data obtained are of relatively inferior quality both because of the low yield (see, e.g., Fig. 1) and because in all but the excitation function spectra, the 83-keV decay of the first-excited state of ^{57}Mn was below the electronic cutoff. Nevertheless, the data are presented here because they substantiate the only previous study[17,18] of γ-ray transitions in ^{57}Mn and because they should be useful in planning more informative studies.

The yrast levels and γ-decay information are presented in Table VIII and the decay scheme deduced from these data is shown in Fig. 6. The spin-parity assignments of Fig. 6 and the branching ratios of Fig. 6 and Table VIII for $E_x < 1500$ keV are from the ^{54}Cr($\alpha, p\gamma$)^{57}Mn results of Mateja *et al.*[18] Our results are fully consistent with these. However, because of relatively very intense ^{57}Fe and ^{59}Co 993-keV transitions, the 1075 → 83 transition could not be observed. Since the 1075 → 0 transition was reported to be only a 6% branch it was not expected to be intense enough to be observed. Thus, we have no direct evidence for the formation of the 1075-keV level. The indirect evidence is the appearance in the γ-ray singles spectra of a 152-keV γ ray which could be the expected ~6% 1228 → 1075 branch. Unfortunately, this γ ray was electronically suppressed in the γ-γ coincidence data and so its assignment is uncertain.

The angular distribution results together with the usual argument favoring formation of yrast levels suggests $J+2 \rightarrow J$ for the 1228 → 83 transition in agreement with the previosuly conjectured spin-parity assignments. $J+1 \rightarrow J$ is also suggested for the 529-keV 3287 → 2758 transition while the DSAM result for the latter constrains this transition to be predominantly dipole.

F. ^{58}Mn

^{58}Mn was formed in the ^{48}Ca(^{13}C, $2np$)^{58}Mn reaction. The peak yield was observed at a bombarding energy of 36 MeV which is consistent with evaporation of three nucleons (see Fig. 1). The γ-γ coincidence matrix for the γ rays assigned to ^{58}Mn is given in Table IX. The assignment of the γ rays of Table IX to ^{58}Mn is based primarily on the ^{13}C + ^{48}Ca excitation function, supported by the nonobservation of any of these seven transitions in the ^{9}Be, ^{11}B, ^{14}N, and ^{18}O bombardment of ^{48}Ca, compared to weak formation of the 376-keV γ ray in ^{15}N + ^{48}Ca. In addition, there is an excellent match in intensity between the proposed ^{58}Mn γ-ray cascade and the ^{58}Mn(β^-)^{58}Fe intensity. The latter was deduced from the ^{13}C + ^{48}Ca in-beam data using the previously deduced decay scheme for this β decay.[11,17]

The only previous spectroscopic information on ^{58}Mn was provided by the ^{58}Fe(t, ^{3}He)^{58}Mn study of Flynn, Sunier, and Ajzenberg-Selove,[19] who reported the decay scheme shown on the left of Fig. 7.

TABLE IX. Summary of γ-γ coincidence data for ^{58}Mn. The intensities of coincident γ-ray pairs are indicated as being relatively strong (S), average (M), or weak (W). Parentheses enclose cases where the observation is so weak as to be uncertain.

E_γ (keV)	144	280	376	579 [a]	581	680	1154	Sum
144	···	W	W	(W)	(W)			W
280	W	···	S	S	M	W	S	S
376		S	···	S	M	M	S	S
580 [a]	(W)	S	S	M	W	M	M	M
680		W	M	W	W	···	(W)	W
1154		S	S	W	W	(W)	···	M

[a] The doublet of 579-581 keV was unresolved in the 2048-channel displayed spectra but not in the 8192-channel gating spectra.

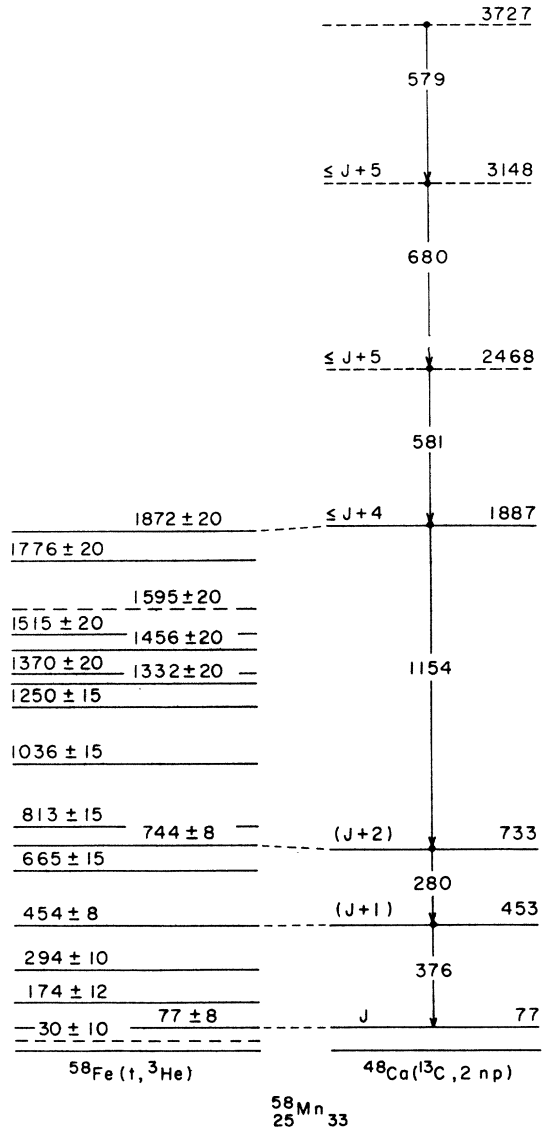

FIG. 7. Level schemes for ^{58}Mn deduced from present studies of the ^{48}Ca(^{13}C,2np)^{58}Mn reaction (right) and previous studies of the ^{58}Fe(t,^{3}He)^{58}Mn reaction (left). The best overlap of the present results with the (t,^{3}He) work is obtained if the lowest-lying level in the observed γ-ray cascade is matched with the 77-keV level, but this assignment is not certain. In addition, the dashed lines for the upper three levels indicate an uncertainty in the ordering.

Usually, the γ-ray decay schemes established via fusion-evaporation in-beam γ-γ coincidence and angular distribution studies end at the ground state. However, this need not be the case when there are one or more low-lying levels whose γ decay may be of too low energy for routine detection. The level scheme proposed by Flynn *et al.*[19] for ^{58}Mn is one such case. Thus, although we can definitely establish the bottom of our decay scheme as $E_0+656\xrightarrow{280}E_0+376\xrightarrow{376}E_0$, where E_0 is the excitation energy (in keV) of a low-lying level of ^{58}Mn, we cannot, from our data alone, say whether E_0 is 0, 30±10, or 77 keV. However, the best overlap of the scheme on the left of Fig. 7 with our γ-ray data is obtained if we assume that $E_0=77$ keV. Our proposed decay scheme, based on this assumption, is drawn on the right in Fig. 7 and is listed in Table X.

Although there was no doubt that the seven listed transitions are in coincidence, it was not possible to place all seven of them unambiguously in a decay scheme: The decay scheme of Fig. 7 and Table X is only one possible choice. The ordering of the 376- and 280-keV γ rays as the two lowest-lying transitions is considered definite. Note that each of these two γ rays is in coincidence with all of the remaining six (see Table X). The placement of the 1154-keV γ ray third in the cascade is almost as certain. This placement follows from the observed Doppler shifts as well as from the intensities. However, the ordering of the 581-, 680-, and 579-keV γ rays is quite uncertain so that the excitation energies of the last three levels of Table X and Fig. 7 are also uncertain.

The lifetime limits determined for the 376-, 280-, and 1154-keV transitions via the RDM (see Table X) establish the lower two as predominantly dipole, since they are too fast to be $E2$ transitions.[7] Likewise, the lifetime limits for the 581- and 680-keV transitions establish them as predominantly dipole and that for the 1154-keV transition restricts it to be dipole or $E2$. The spin restrictions shown in Fig. 7 follow from these limits together with the fact that the angular distributions of the 376- and 280-keV transitions are characteristic of predominantly dipole $J\pm1\rightarrow J$ transitions and the reaction mechanism favors $J+1$ over $J-1$.

For the five higher-lying transitions, the angular distributions and intensities were determined only poorly, if at all, mainly due to the relative weakness for formation of ^{58}Mn in ^{13}C+^{48}Ca. In the singles spectra, the Doppler-shifted 581-keV γ ray was unresolved from the 579-keV γ ray and from a contaminant 579-keV peak whose yield peaked at >65 MeV. Likewise the Doppler-broadened 680-keV γ ray was unresolved from a 680-keV contaminant with a yield still rising at 65 MeV. Finally the 1153-keV peak was incompletely resolved from the much more intense and Doppler-broadened 1158-keV transitions of ^{57}Fe.

In the ^{58}Fe(t,^{3}He)^{58}Mn studies of Flynn *et al.*[19] the most energetic ^{3}He group was relatively weak and broader than expected for a single level. Thus, it is possible (but unlikely) that this group[19]

TABLE X. Proposed placement of γ rays observed in the ^{48}Ca(^{13}C, $2np$)^{58}Mn reaction at $E(^{13}C) = 40$ MeV.

E_i [a] (keV)	E_f (keV)	E_γ (keV)	Angular distribution [b] (I_γ)	A_2 (%)	$F(\tau)$ [c]	τ [d] (ps)
453.45(10)	77	376.45(10)	28 650	−69(2)	<0.30	<50
733.28(16)	453	279.83(12)	20 145	−39(2)	<0.50	<50
1886.83(25)	733	1153.54(20)	15 000	···	<0.50	>0.6, <50
2468.26(32)	1887	581.43(20)	~10 000	···	>0.50	<0.6
3148.29(39)	2468	680.03(23)	~5 000	···	>0.70	<0.4
3727.30(50)	3148	579.01(30)	~5 000	···	···	···
?	?	144.13(15)	~6 000	···	<0.50	>0.6

[a] The level energies are calculated assuming the observed γ-ray cascade (column 3) ends at a 77.00-keV level (see text) from the γ-ray energies of column 3 including the nuclear recoil correction. The order of the last three listed γ rays (and thus the existence of the 2468- and 3148-keV levels) is uncertain (see text). The numbers in parentheses throughout the table are the uncertainties in the least significant figure.

[b] The γ-ray angular distribution is given by $W(\theta) = I_\gamma[1 + A_2 P_2(\cos\theta) + A_4 P_4(\cos\theta)]$. The A_4 coefficients were not determined with sufficient accuracy to distinguish them from zero.

[c] The DSAM attenuation factor defined in Ref. 1.

[d] Limit on the mean life of the level (E_i) extracted from the RDM for the first two listed levels and from $F(\tau)$ for the remainder (see text).

is not due to ^{58}Mn so that the level identified as $E_x = 77$ keV is actually the ground state. Flynn *et al.* speculated that this group, because of its breadth, was due to a doublet; hence the speculated, but uncertain level at 30 ± 10 keV. If this latter level does not exist, then the excitation energies of ^{58}Mn (Fig. 7) should all be lowered by 15.00 keV. In our measurements a 77 ± 8 keV transition with an intensity $>\frac{1}{2}$ that of the 376-keV γ ray was not present. However, because of the very intense x rays from the Ta backing of the ^{48}Ca target, a ^{58}Mn peak in the energy region 55–68 keV would not have been observed. In any case, the match in intensities between the 376-keV γ transition and the 66-sec β feeding of ^{58}Fe assures us that the β-emitting $J^\pi = (3)^+$ level of ^{58}Mn (Ref. 17) is the bottom level in the yrast decay of ^{58}Mn. An experiment designed to search for a low-energy transition ($50 \lesssim E_\gamma \lesssim 70$ keV) in cascade with the γ rays of Table IX would appear to be most appropriate.

III. DISCUSSION

As part of our broad survey of high-spin states in fp-shell nuclei, we have performed shell-model calculations using the Oak Ridge-Rochester shell-model code.[20] A closed ^{48}Ca core was assumed, and active protons were confined to the $1f_{7/2}$ shell and active neutrons to the $1f_{5/2}$, $2p_{3/2}$, and $2p_{1/2}$ shells; i.e., we assumed the configurational space

$$[\pi(1f_{7/2})^{-n} \otimes \nu(2p_{3/2}, 1f_{5/2}, 2p_{1/2})^m], \qquad (1)$$

where $n = 28 - Z$ and $m = N - 28$. A modified surface δ interaction was chosen to calculate the n-p matrix elements. Except for ^{58}Fe, only level positions were calculated and not transition rates or static moments. References to previous shell-model calculations are given in I.

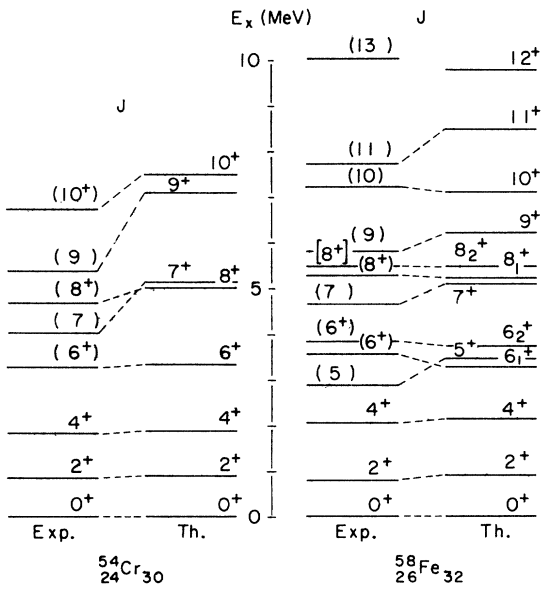

FIG. 8. Comparison of experimental observations and theoretical predictions for the yrast states of ^{54}Cr and ^{58}Fe. The calculations utilize the ORNL-Rochester shell-model code and assume a closed ^{48}Ca core. The experimental data are from the present work.

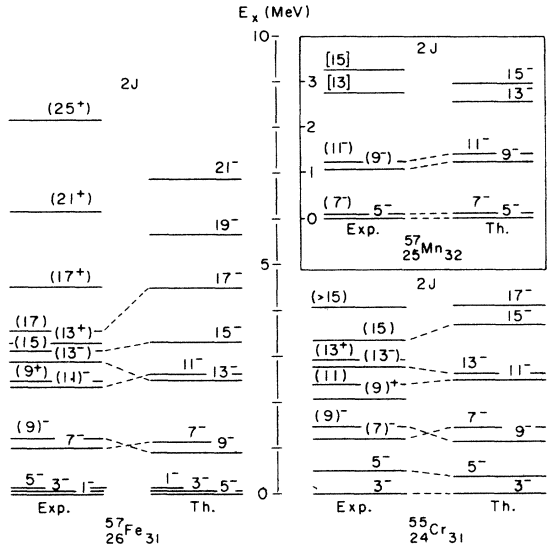

FIG. 9. Comparison of experimental observations and theoretical predictions for the yrast and near-yrast states of ^{57}Fe, ^{57}Mn, and ^{55}Cr. Also shown are the experimental positive-parity levels which lie outside the configuration space of the calculation.

Comparisons between the theoretical and experimental spectra (except for ^{58}Mn, which was not calculated) are shown in Figs. 8 and 9. With a few exceptions, only the yrast levels are shown. For the even-A nuclei (Fig. 8), there is generally a good one-to-one correspondence between the calculated and experimental levels. The agreement is particularly good for states of even J, while for odd J the theoretical predictions appear to be systematically too high. Note also that the $J = (13)$ state in ^{58}Fe lies outside the configurational space of (1). We will further discuss the spectra and transition rates in ^{54}Cr and ^{58}Fe below. For the odd-A nuclei (Fig. 9), the situation is somewhat more complicated. Although ^{57}Mn seems to be well accounted for by the calculation, the ordering of the yrast levels is not correctly predicted in ^{55}Cr and ^{57}Fe. Further, the appearance of positive-parity levels in these latter two nuclei signals the excitation of one or more nucleons out of the configuration specified by (1) and into the $1g_{9/2}$ orbital. We will examine this point in greater detail below as we now discuss specific points of interest for the various nuclei.

A. ^{54}Cr

As discussed in Sec. II C, the even-J yrast levels in ^{54}Cr consist of a $\Delta J = 2$ sequence extending from the 0^+ ground state to the 10^+ level at 6720 keV. The level spacings are well reproduced by the shell-model calculations (Fig. 8) and are suggestive of a rotational behavior. Both the experimental and theoretical $E2$ enhancements, which are compared in the last two columns of Table V, lend additional support to this picture. The present calculations are in basic agreement with the earlier but less extensive work of Horie and Ogawa.[21,22] It has been noted by Bhatt, Parikh, and McGrory[23] and more recently by Ogawa[24] that because of the quadrupole-quadrupole ($Q \cdot Q$) dominance of the residual n-p interaction, the yrast and near-yrast states of ^{54}Cr are composed of quite simple shell-model configurations. That is, when one computes the n-p matrix elements in a weak coupling basis $[^{52}\mathrm{Cr}(\pi^4) \otimes {}^{58}\mathrm{Ni}(\nu^2)]$ and then diagonalizes the energy matrix, one finds that a considerable truncation of the configuration space is possible since only neutron and proton configurations with large diagonal and off-diagonal matrix elements of the quadrupole operator need be included. For example, only the lowest 0^+, 2^+, and 4^+ two-neutron states of ^{58}Ni are important in the ^{54}Cr calculation. In recent calculations of the yrast states in ^{54}Cr using such a truncated space,[23,24] it has been shown that the resulting spectrum agrees quite well with both the more exact calculation and the present experimental data.

As an example of the importance of n-p correlations in determining the spectrum of ^{54}Cr, consider the lowest 2^+ states. In the absence of n-p correlations, the weak coupling states are approximate eigenstates and one would therefore expect two nearly degenerate 2^+ states at $\simeq$1400 keV, both of which have about equal $E2$ strengths to the ground state. The $Q_n \cdot Q_p$ force nearly completely mixes these states, pushing them apart and giving most of the ground-state $E2$ strength to the lower one. In this way one sees that it is the n-p correlations that give rise to the collective rotational-like behavior. This concept is not new,[25] of course, nor is its application to ^{54}Cr unique. Similar behavior has already been noted in ^{56}Fe (Refs. 24 and 26) and should equally well apply to ^{58}Fe and ^{60}Fe.

B. ^{58}Fe

The $\Delta J = 2$ yrast band in ^{58}Fe displays a level spacing (at least through the 8^+ level) very similar to that in ^{54}Cr. However, the interesting feature here is the appearance of closely spaced doublets for both the 6^+ and 8^+ levels. This seems to be well accounted for by the calculation (Fig. 8), and it is useful to examine more closely the nature of these doublets. In Table XI we list the calculated quadrupole moments of the yrast states and the $B(E2)$'s connecting these states. It is apparent from both the predicted sign change of the quadrupole moment of the 8^+ state and the greatly dimin-

TABLE XI. Calculated quadrupole moments and $B(E2)$'s for yrast levels in ^{58}Fe. Effective charges of $e_p = 2.0$ and $e_n = 1.0$ are assumed.

J_i^π	J_f^π	Q_i (e fm^2)	$B(E2; f \to i)$ (W.u.)
2^+	0^+	−27	16.9
4^+	2^+	−25	17.5
6^+	4^+	−24	19.6
8^+	6^+	+47	0.7
10^+	8^+	+29	0.9
12^+	10^+	+15	1.8

ished $B(E2; 8_1^+ \to 6_1^+)$ that a change in nuclear shape occurs between the 6^+ and 8^+ levels. Experimentally, the primary evidence for such a shape transition is the preference for the 8_1^+ state to decay to the second 6^+ state rather than the first (see Table IV) and the fact that $B(E2; 6_2^+ \to 4_1^+)/B(E2; 6_1^+ \to 4_1^+) < 0.06$. All this is quite suggestive of a band-crossing phenomenon, whereby the yrast states are the states in the prolate-deformed ($Q < 0$) ground-state band through the 6^+ level but the 8^+ member of this band lies above the yrast 8^+ level, which is oblate-deformed ($Q > 0$). One obvious discrepancy with experiment, however, is in the sign[27] of $Q_{2_1^+}$; in view of its importance in understanding the spectrum of ^{58}Fe, we suggest a remeasurement of this quantity.

It is interesting that the calculations predict a similar prolate-to-oblate transition in both ^{56}Fe and ^{60}Fe. This phenomenon has already been observed to occur between the 4_1^+ and 6_1^+ levels in ^{56}Fe (Ref. 26) as predicted, but there is as yet insufficient data[2] to confirm the effect in ^{60}Fe. Finally, we note that the coexistence in this mass region of both prolate and oblate states at relatively low excitation has been predicted by Hartree-Fock calculations of Parikh.[28]

C. ^{57}Fe and ^{55}Cr

The outstanding feature of these spectra is the appearance of a low-lying $\Delta J = 2$ positive-parity band built upon a $J^\pi = \frac{9}{2}^+$ level. Although observed in both the present ^{55}Cr data and the previously reported ^{59}Fe spectrum,[2] this band is especially apparent in ^{57}Fe, where it extends up to a suggested $\frac{25}{2}^+$ level and where the band members are connected by enhanced $E2$ transitions. This is demonstrated in Fig. 10, which also shows the remarkable similarity of the level spacings and $B(E2)$'s to those of the ground-state band in ^{56}Fe. All this suggests the coupling of a $1g_{9/2}$ neutron to a ^{56}Fe core, and it is the nature of this coupling that we will now examine.

A simple weak-coupling scheme would account

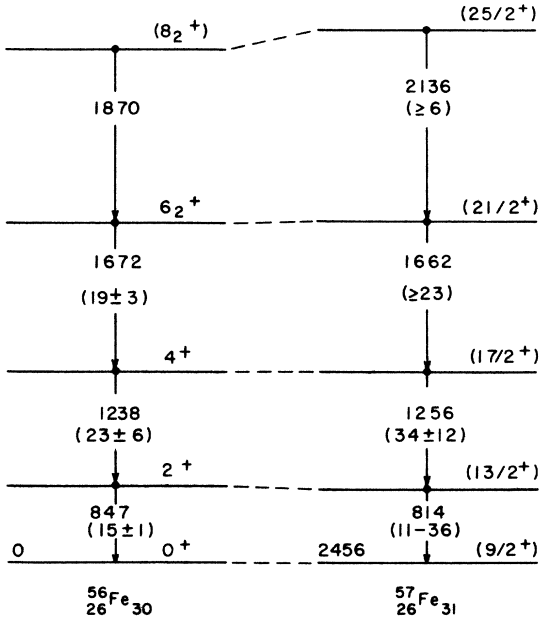

FIG. 10. Comparison of the level spacings and $B(E2)$'s (given in parentheses) between the ground-state band of ^{56}Fe and the $\Delta J = 2$ positive-parity band in ^{57}Fe built upon the $J^\pi = \frac{9}{2}^+$ level at 2456 keV. The data for ^{56}Fe are from Ref. 26.

for the observed level spacing and enhanced $B(E2)$'s but offers no explanation for the missing levels in each multiplet (e.g., those with $J^\pi = \frac{11}{2}^+$, $\frac{15}{2}^+$, etc.). An alternative explanation, as originally proposed by Stephens *et al.*[29] to explain a similar phenomenon in the odd-A La isotopes, is the coupling of a single neutron in a unique parity, high-j orbital (the $1g_{9/2}$ orbital) to a moderately deformed prolate core (^{56}Fe). Under these conditions, it is straightforward to show that the Coriolis force tends to mix the Nilsson projections in such a way as to align the angular momentum of the odd neutron in the direction of the rotation of the core, thus decoupling the two motions. Consequently a so-called rotation-aligned or decoupled band is formed with $J = J_{\text{core}} + \frac{9}{2}$ and with the level spacing of the rotating core.[30] The "stretched-minus-one" levels ($J = J_{\text{core}} + \frac{9}{2} - 1$) are pushed above the corresponding stretched states by the diagonal Coriolis matrix elements and are therefore suppressed from the present data by the reaction mechanism. Finally the $B(E2)$'s of the resulting nucleus are quite simply related to those of the core.[30] Thus although the experimental $B(E2)$'s are not precise enough to allow a detailed comparison, this rotation-aligned coupling scheme seems to quite nicely account for the ^{57}Fe data. We note that had the ^{56}Fe core been oblate, then this model would predict a strongly coupled K^π

$=\frac{9}{2}^+$ band with the normal level sequencing.

It has been pointed out[31,32] that the occurrence of such decoupled bands is not limited to axial rotors and indeed is a much more widespread phenomenon. All one need assume is a $Q \cdot Q$ interaction between the odd nucleon and the core. Then, depending only on the sign of the product of quadrupole moments, one can generate either a decoupled band or a strongly coupled band nearly independently of the details of the particular nucleus. Thus, decoupled bands have been observed in a wide range of nuclei from deformed rotors[29] to anharmonic vibrators.[32]

D. Summary

It is rather pleasing that several interesting features of *fp*-shell nuclei, as exemplified by those nuclei studied here, can be described in terms of a few simple and very basic ideas. First, the *n-p* correlations determine to a large extent the collective behavior of the even-even nuclei in this region, and lead to a quite simple prescription for the truncation of the configuration space, at least for the yrast and near-yrast levels. Further, the "backbending" phenomena observed in the even-*A* iron isotopes has as a natural explanation the crossing of oblate and prolate bands. And finally, we see evidence in some of the odd-*A* nuclei for the existence of decoupled bands built upon the unique parity $g_{9/2}$ orbital. It will be interesting to see if these effects persist as more spectroscopic information becomes available for other nuclei in this mass region.

We acknowledge several useful discussions with Professor I. Talmi and Dr. F. Iachello. We would also like to thank Dr. J. Delaunay for communicating results on ^{58}Fe prior to publication.

Note added in proof. The results of Ref. 10 have now been published: S. Cavallaro, J. Delaunay, R. Ballini, T. Nomura, N. Bendjaballah, and C. Tosello). Nucl. Phys. A293, 125 (1977). Our results appear to be in general agreement with theirs, although discrepancies are evident in some of the lifetimes reported from the two sets of experiments.

---

†Research supported by the Department of Energy under Contract No. EY-76-C-02-0016.

*Present address: Physics Department, University of Illinois, Urbana, Illinois 61801.

‡Research sponsored by the U. S. Energy Research and Development Administration under contract with Union Carbide Corporation.

[1]A. M. Nathan, J. W. Olness, E. K. Warbuton, and J. B. McGrory, Phys. Rev. C 16, 192 (1977).
[2]E. K. Warburton, J. W. Olness, A. M. Nathan. J. J. Kolata, and J. B. McGrory, Phys. Rev. C 16, 1027 (1977).
[3]Z. P. Sawa, Phys. Scr. 6, 11 (1972).
[4]R. L. Auble, Nucl. Data Sheets 20, 327 (1977).
[5]G. A. P. Engelbertink, L. P. Ekström, D. E. C. Scherpenzeel, and H. H. Eggenhuisen, Nucl. Instrum. Methods 143, 161 (1977).
[6]E. K. Warburton, J. J. Kolata, J. W. Olness, A. R. Poletti, and Ph. Gorodetzky, At. Data Nucl. Data Tables 14, 147 (1974).
[7]P. M. Endt and C. Van der Leun, At. Data Nucl. Data Tables 13, 1 (1974).
[8]H. M. Sen Gupta, A. R. Majumder, and E. K. Lin, Nucl. Phys. A160, 529 (1977).
[9]J. A. Thomson, Nucl. Phys. A227, 485 (1974).
[10]J. Delaunay (private communication).
[11]D. C. Kocher and R. L. Auble, Nucl. Data Sheets 19, 445 (1976).
[12]A. M. Nathan, D. E. Alburger, J. W. Olness, and E. K. Warburton, Phys. Rev. C 16, 1566 (1977).
[13]Nuclear Data Group, Nucl. Data Sheets (to be published).
[14]D. C. Kocher, Nucl. Data Sheets 18, 463 (1977).
[15]A. E. Macgregor and G. Brown, Nucl. Phys. A198, 237 (1972).
[16]D. M. Rosalky, D. J. Baugh, J. Nurzynski, and B. A. Robson, Nucl. Phys. A142, 469 (1970); R. Bock, H. H. Duhm, S. Martin, R. Rüdel, and R. Stock, *ibid.* 72, 273 (1965).
[17]K. G. Tirsell, L. G. Multhauf, and S. Raman, Phys. Rev. C 10, 785 (1974).
[18]J. F. Mateja, G. F. Neal, J. D. Goss, P. R. Ghagnon, and C. P. Browne, Phys. Rev. C 13, 118 (1976).
[19]E. R. Flynn, J. W. Sunier, and F. Ajzenberg-Selove, Phys. Rev. C 15, 879 (1977); and private communication from F. Ajzenberg-Selove.
[20]J. B. French, E. C. Halbert, J. B. McGrory, and S. S. M. Wong, in *Advances in Nuclear Physics*, edited by M. Baranger and E. Vogt (Plenum, New York, 1969), Vol. 3.
[21]H. Horie and K. Ogawa, Nucl. Phys. A216, 407 (1973).
[22]H. Horie and K. Ogawa, Prog. Theor. Phys. 46, 439 (1971).
[23]K. H. Bhatt, J. K. Parikh, and J. B. McGrory, Nucl. Phys. A224, 301 (1974).
[24]K. Ogawa, Phys. Rev. C 15, 2209 (1977).
[25]R. K. Sheline, Rev. Mod. Phys. 32, 1 (1960).
[26]N. Bendjaballah, J. Delaunay, A. Jaffrin, T. Nomura, and K. Ogawa, Nucl. Phys. A284, 513 (1977); D. G. Sarantites, J. Urbon, and L. L. Rutledge, Jr., Phys. Rev. C 14, 1412 (1976).
[27]C. W. Towsley, Ph.D. thesis, Rochester Univ., 1974 (unpublished).
[28]J. K. Parikh, Phys. Rev. C 10, 2568 (1974).
[29]F. S. Stephens, R. M. Diamond, J. R. Leigh, T. Kammuri, and K. Nakai, Phys. Rev. Lett. 29, 438 (1972).
[30]F. S. Stephens, Rev. Mod. Phys. 47, 43 (1975).
[31]I. Talmi (private communication); F. Iachello (private communication).
[32]G. Alaga and V. Paar, Phys. Lett. 61B, 129 (1976).